A Novel Screening Assay for Activation State-Selective Kinase Inhibitors Based on Ion Mobility-Mass Spectrometry

Jessica N. Rabuck[1], Suk-Joon Hyung[1], Kristin S. Ko[2], Christel C. Fox[2], Matthew B. Soellner[1,2],*

*Brandon T. Ruotolo[1]**

[1]Department of Chemistry and [2]Department of Medicinal Chemistry, University of Michigan,

930 N. University Ave., Ann Arbor, MI 48109

SUPPORTING INFORMATION

SI Text

On the Origin of CIU Fingerprint bands

We state that our CIU fingerprints contain bands that originate from multiple processes that occur upon the coalitional activation of Abl-inhibitor complexes. All of these transitions generate mass-resolvable features that we can track independently to determine their relative influence on the composite fingerprints we use to differentiate type I and II inhibitor complexes (**Figure S1**). Both composite and individual fingerprint contributions for tozasertib (type I) and ponatinib (type II) indicate that while inhibitor stripping and charge reduction (which predominately occurs with concomitant inhibitor loss) both occur at relatively low voltage values to some extent, both populations of ions also undergo unfolding (as indicated by the larger drift times achieved for each individual ion population shown). In general, inhibitor and charge stripped species tend to give rise to many of the CIU features recorded at high collision voltages. Thus their inclusion within our composite screening approach is critical to its success, as we identify this region as the most differentiating between different inhibitor classes.

Average Drift Time Spectra for Three CIU Regions

In determining the area within CIU fingerprints that provide the maximum level of discrimination between type I and type II kinase inhibitors, we evaluated three principle voltage ranges: 20-28V, 32-36V, and 40-44V. These three regions were selected for detailed analysis based on a visual inspection of CIU fingerprints for Abl-inhibitor complexes, and preliminary data for 10^{+} protein-inhibitor complexes shown in Figure 3 (main text). As such, we computed the average IM drift time spectra for all three regions and compared both the number of unique features detected, the resolving power achieved, and the total number of peaks observed (**Figure**

S3). The IM data collected between 20V and 28V, while useful for differentiating imatinib and dasatinib complexes in Figure 3, contains only two features on average, with only 1 feature having a unique centroid value for each type I and II averaged IM spectrum. This, combined with the relatively poor peak resolution within this region makes it a non-optimized choice for differentiating type I and I inhibitors in a broad dataset. Intermediate voltage regions show two well-resolved peaks for the average type II CIU response, and three poorly-resolved features for type I-bound complexes, with both sets being mutually exclusive to their respective datasets. High voltage data provides the largest number of peaks for type II average data (5 resolved features and one shoulder), all with unique centroid drift times when compared with the two main features recorded for the average type I CIU response. The superior discriminating power of this final higher-voltage region of our CIU data is supported by the similarity scores calculated in **Supplemental Tables 1 and 2**. In **Supplemental Table 2** specifically, we use other methodologies to calculate a score value useful for screening. For example, we attempt to normalize our scores to the average type I and type II signatures, rather than to a maximum type II response. While we find some of these methods to provide strong discrimination power, none seem substantially superior to the approach indicated in the main text (Table 1).

Simple IM Separations are Insufficient to Differentiate between Type I and Type II Binders in Complex with the Abl Kinase Domain.

Our initial approach to differentiate type I and II kinase inhibitors using IM separation included a simple separation strategy that relies exclusively on the orientiationally-averaged collision cross-section (CCS) difference between the two bound states of the protein to generate differentiated responses. We found that the two bound states differ, at most, by IM drift time values of 2.5%,

which correlates to a ~1.5% difference in CCS (**Figure S4**). This correlates well to the difference in the projected areas (PA) calculated for the two X-ray structures of the proteins bound to the same inhibitors (PDB ID: 1IEP for imatinib-bound Abl, and PDB 2GQG for dasatinib-bound Abl), which predicts a CCS difference of 1% for the gas-phase ions [1]. We also note that both of these bound states are, interestingly, somewhat larger (~4-6%) than the apo form of the protein in the gas-phase.

Extrapolating Type II similarity scores to a larger chemical library screen.

The 11 compounds used to train our IM-MS approach represent all of the commercially obtainable inhibitors available where there is strong structural evidence that identifies the kinase binding mode involved. While this dataset is small in comparison to a typical library screen, we felt it instructive to use the mean and standard deviations of our current dataset to graphically project the type I and II responses expected for an 1800 compound inhibitor library comprised equally of type I and II inhibitors. In this scenario, depicted in **Figure S5**, while overlap exists between the two scoring ranges identified in this report for the two inhibitor classes, type II compounds having strong similarity scores are easily distinguished from type I inhibitors, which tend to cluster more strongly in our measurement. Depending upon the stringency of the screen employed, false positive values from the CIU-based approach can be tuned to nearly zero, if desired.

Phosphorylation of c-Abl. c-Abl was phosphorylated following a previously described procedure.[1,2] Briefly, since c-Abl is inefficient at autophosphorylation, it was incubated with hematopoietic cell kinase (Hck) at room temperature for 1 hour in Buffer D (50 mM Tris (pH

8.0), 100 mM NaCl, 5% glycerol, and 1 mM DTT), 30 mM $MgCl_2$, 10 μM c-Abl, 5 mM ATP, 100 μM Na_3VO_4, and 50 nM Hck and passed through a Sephadex G25 column eluting with Buffer D.

General procedure for ATP K_m determination. The previously described fluorescence assay[3] was used to determine K_m values. Reaction volumes of 100 μL were used in 96-well plates. 85 μL of enzyme in buffer was added to each well. 2.5 μL of DMSO was then added followed by 2.5 μL of substrate peptide (AEXIYAAPF-OH, where X is 2,3-diaminopropionic acid) solution (1.8 mM in DMSO). The reaction was initiated with 10 μL of the appropriate ATP dilution (typically 1000, 500, 250, 125, 62.5, 31.3, 15.6, 7.8, 3.9, 2.0 μM in H_2O) and reaction progress was immediately monitored at 405 nm (ex. 340 nm) for 10 minutes. Reactions had final concentrations of 100 nM enzyme, 45 μM peptide substrate, 100 μM Na_3VO_4, 100 mM Tris buffer (pH 8), 10 mM $MgCl_2$, 0.01% Triton X-100. The initial rate data collected was used for determination of K_m values. For K_m determination, the kinetic values were obtained directly from nonlinear regression of substrate-velocity curves in the presence of varying concentrations of ATP. The equation Y = (Vmax * X)/(Km + X), X = substrate concentration (μM) and Y = enzyme velocity (RFU/s); was used in the nonlinear regression. Each ATP K_m value was determined using at least three independent experiments; a representative K_m curve is shown for both phosphorylated and nonphosphorylated c-Abl (**Figure S8 and S9)**.

General procedure for determination of inhibitor K_i for Phosphorylated and Non-Phosphorylated c-Abl: c-Abl inhibition assay was performed using a continuous, fluorimetric assay as previously described.[3] Reaction volumes of 100 μL were used in 96-well plates. To each

well was added 85 μL of buffer + enzyme. 2.5 μL of varying concentrations of inhibitor was then added (typically 10000, 2500, 625, 156, 39, 10, 2.4, 0.61, 0.15, 0 μM in DMSO). 2.5 μL of peptide substrate (AEXIYAAPF-OH, where X is 2,3-diaminopropionic acid) solution (1.8 mM in DMSO) solution was added. 10 μL of ATP (50 mM in water) was added to initiate the reaction and was immediately monitored at 405 nm (ex. 340 nm) for 10 minutes. Final concentrations in the reaction are 100 nM enzyme, 45 μM peptide substrate, 5 mM ATP, 100 μM Na_3VO_4, 100 mM Tris buffer (pH 8), 10 mM $MgCl_2$, 0.01% Triton X-100. The initial rate of the reaction was used to determine K_i values. For K_i determination, the kinetic values were obtained directly from nonlinear regression of substrate-velocity curves in the presence of various concentrations of the inhibitor. The equation Y = Bottom + (Top – Bottom)/1 + 10^{x} – $LogEC_{50}$), X = log(concentration) and Y = binding; was used in the nonlinear regression.

Mass spectrometry of Apo Abl and P-Abl. Apo Abl and phosphorylated (P)-Abl samples were buffer exchanged into 200 mM ammonium acetate using Micro Bio-Spin 6 columns (Bio-Rad, Hercules, CA) and prepared into a final concentration of 12 μM. Sample aliquots (~5μl) were analyzed on a Q-IM-TOF MS instrument (Synapt G2 HDMS, Waters, Milford, Ma) and ionized using a nESI source, in a manner similar to that described above. The capillary voltage was held at 1.2 kV, with the source operating in positive mode, the sample cone operating at 65V, the extraction cone operating at 6V, and the TCE operating at 20V to aide desolvation and accurate mass determination. The average mass of ApoAbl was measured to be 33182.38 ±0.88Da, while 33261.88 ±0.18Da was recorded for P-Abl. The difference between the two masses is 79.52 ±0.90Da, indicating that the protein is fully phosphorylated. A small amount (less than 10%) of Apo Abl was detected in some P-Abl MS data (**Figure S10**).

References

1. Nagar, B. et al. Crystal Structures of the Kinase Domain of c-Abl in Complex with the Small Molecule Inhibitors PD173955 and Imatinib (STI-571). Cancer Research 62, 4236-4243 (2002).
2. Schindler, T. et al. Structural Mechanism for STI-571 Inhibition of Abelson Tyrosine Kinase. Science, 289, 1938-1942 (2000).
3. Wang, Q.; Cahill, S. M.; Blumenstein, M.; Lawrence, D. S. Self-Reporting Fluorescent Substrates of Protein Tyrosine Kinases. J. Am. Chem. Soc. 1808-1809 (2006).

Table S1

Supplemental Table 1. CIU based similarity scores

		Region1: Trap Collision energy 40-44V				Region2: Trap Collision energy 32-36V				Region1: Trap Collision energy 20-28V			
Drugs	type	χ^2 Value for drug and average type I	χ^2 Value for drug and average type II	Normalized type I similarity score	Normalized type II similarity score	χ^2 Value for drug and average type I	χ^2 Value for drug and average type II	Normalized type I similarity score	Normalized type II similarity score	χ^2 Value for drug and average type I	χ^2 Value for drug and average type II	Normalized type I similarity score	Normalized type II similarity score
Imatinib	II	2311.921	155.467	15.81	100	505.61	145.82	71.63	100	253.79	127.05	13.28	100
Nilotinib	II	563.26	210.37	64.91	73.90	481.20	143.83	75.26	101.38	100.58	142.55	33.50	89.13
Ponatinib	II	540.72	251.19	67.62	61.89	159.83	379.37	226.59	38.44	106.65	106.65	31.60	119.13
Sorafenib	II	254.97	319.98	143.42	48.59	344.37	10340.1	105.08	1.41	131.71	1279.12	25.60	9.93
DCC-2036	II	247.09	358.28	147.98	43.40	197.86	455.63	183.04	32.00	241.45	234.82	13.96	54.11
Bosutinib	I	150.01	365.51	243.75	42.53	246.68	18241.89	146.82	0.80	222.08	229.33	15.18	55.4
Tozasertib	I	113.80	368.26	321.30	42.21	75.19	1264.73	481.66	11.53	48.28	31.84	69.70	399.03
PP2	I	246.62	389.67	148.25	38.89	523.36	1483.46	69.20	9.83	315.17	418.12	10.69	30.39
Saracatinib	I	486.57	442.21	75.15	35.16	485.38	634.82	74.61	22.97	328.32	642.12	10.26	19.79
Staurosporine	I	218.46	634.61	167.37	24.50	139.73	2367.54	259.18	6.16	126.92	1377.02	26.56	9.22
Dasatinib	I	365.64	939.87	100	21.75	362.163	156.24	100	93.33	33.70	22.79	100	557.50

Table S2

Supplemental Table 2. CIU based similarity scores validation

Region1: Trap Collision energy 40-44V				
Drugs	type	Normalized type I score	Normalized type II score	Ratio type II/type I
Imatinib	II	8.99	152.77	16.99
Nilotinib	II	36.90	112.76	3.06
Ponatinib	II	38.47	94.34	2.45
Sorafenib	II	81.79	74.00	0.90
DCC-2036	II	84.10	66.14	0.79
Bosutinib	I	138.5	64.70	0.47
Staurosporine	I	95.30	37.35	0.39
PP2	I	84.45	48.42	0.57
Saracatinib	I	42.75	53.57	1.25
Tozasertib	I	182.24	64.34	0.35
Dasatinib	I	56.76	25.19	0.44

Region2: Trap Collision energy 32-36V				
Drugs	type	Normalized type I score	Normalized type II score	Ratio type II/type I
Imatinib	II	37.98	182.99	4.42
Nilotinib	II	39.91	185.52	4.65
Ponatinib	II	120.16	70.34	0.59
Sorafenib	II	55.72	2.58	0.05
DCC-2036	II	97.06	58.56	0.60
Bosutinib	I	77.85	1.46	0.02
Staurosporine	I	137.44	11.27	0.08
PP2	I	36.69	17.99	0.49
Saracatinib	I	39.57	42.03	1.06
Tozasertib	I	255.42	21.10	0.08
Dasatinib	I	53.03	170.79	3.22

Region1: Trap Collision energy 20-28V				
Drugs	type	Normalized type I score	Normalized type II score	Ratio type II/type I
Imatinib	II	34.27	134.30	3..92
Nilotinib	II	86.48	119.70	1.38
Ponatinib	II	81.55	159.99	1.96
Sorafenib	II	66.04	13.34	0.20
DCC-2036	II	36.02	72.67	2.02
Bosutinib	I	39.16	74.41	1.90
Staurosporine	I	68.53	12.39	0.18
PP2	I	27.60	40.81	1.48
Saracatinib	I	26.49	26.57	1.00
Tozasertib	I	180.14	535.91	2.98
Dasatinib	I	258.08	748.73	2.90

Normalized type I equation:

$$\frac{\frac{A1}{\chi^{2,1}}x100}{B}x100$$

A1 is the average type I score for type I drugs
$\chi^{2,1}$ is the type I χ^2 value
B is averaged A1 value for type I drugs

Normalized type II equation:

$$\frac{\frac{C1}{\chi^{2,2}}x100}{D}x100$$

B1 is the average type I score for type I drugs
$\chi^{2,2}$ is the type II χ^2 value
D is averaged C1 value for type II drugs

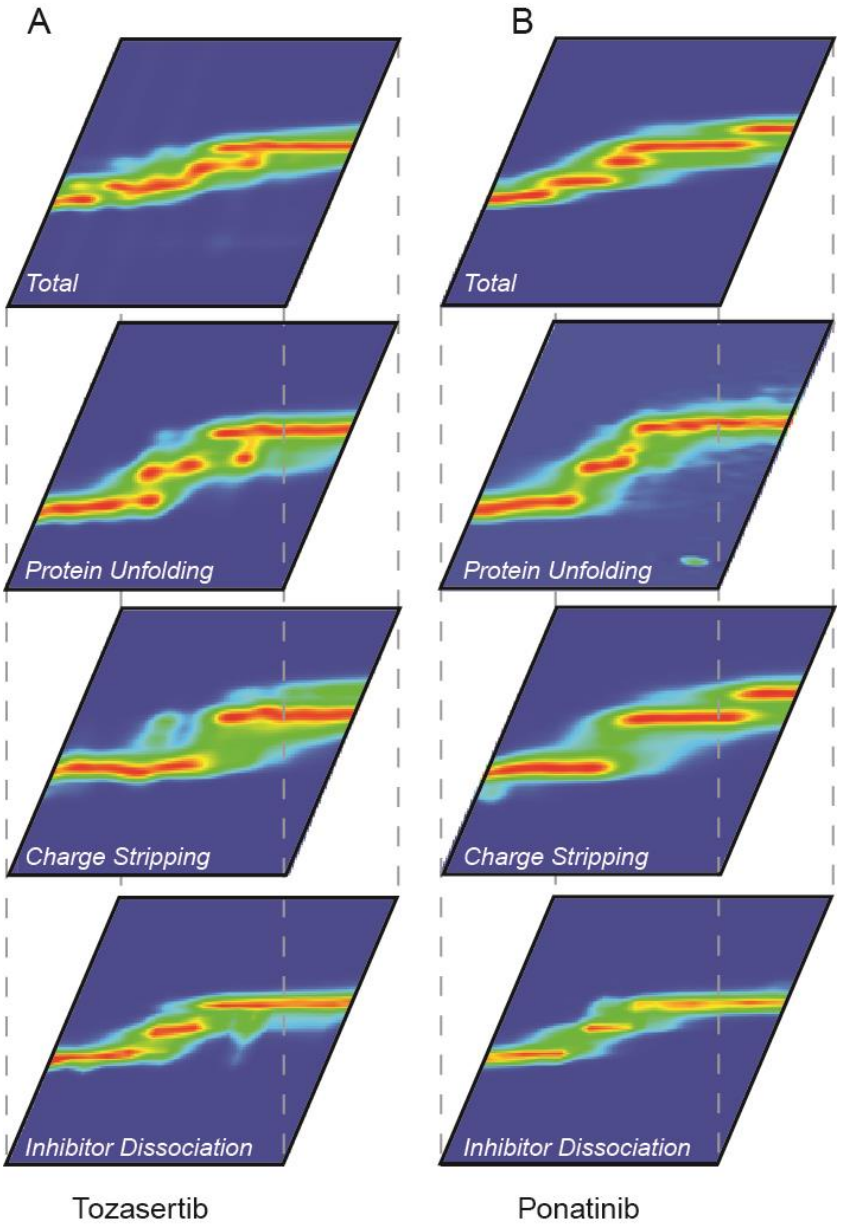

Figure S1. Individual mass-resolved components of the CIU fingerprints for Abl-inhibitor complex. The CIU data is shown for m/z values corresponding to inhibitor dissociation (bottom), charge stripping/inhibitor dissociation (bottom- middle) and protein unfolding (top-middle) for the intact protein-inhibitor complexes of Abl bound to (**A**) Tozasertib (type I) and (**B**) Ponatinib (type II).

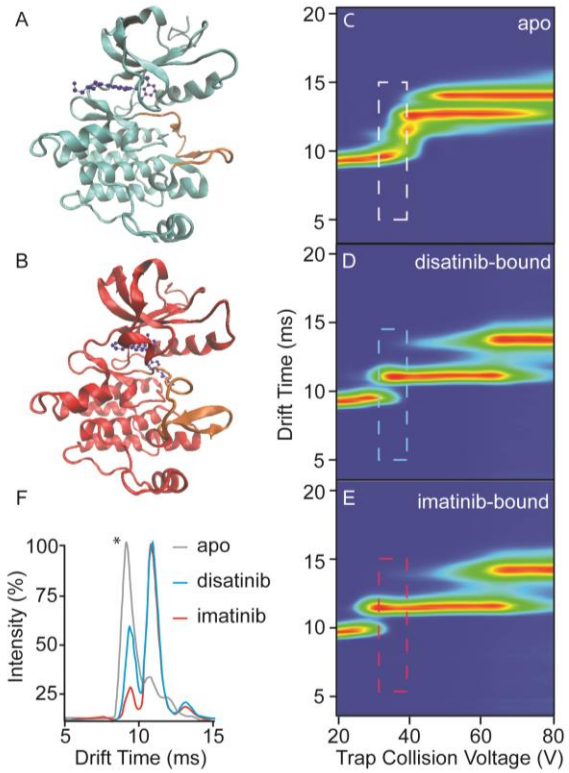

Figure S2. X-ray structures (1IEP) for Abl bound to dasatinib (**A**) shown in blue, and imatinib (**B**) shown in red. The activation loop (orange) changes between the two structures. CIU fingerprints derived from 10^{+} ions corresponding to Apo-Abl kinase (**C**), Abl bound to dasatinib (**D**) and Abl bound to imatinib (**E**). The dashed boxes highlight a potential region of the plot useful for high-throughput screening, and are color coded to match the other sections of the figure. Drift time plot from the three dashed-box regions in C-E (**F**), a factor of 2.5 fold difference in compact protein conformer intensity (*) is observed between the two inhibitor data-sets (colors as indicted).

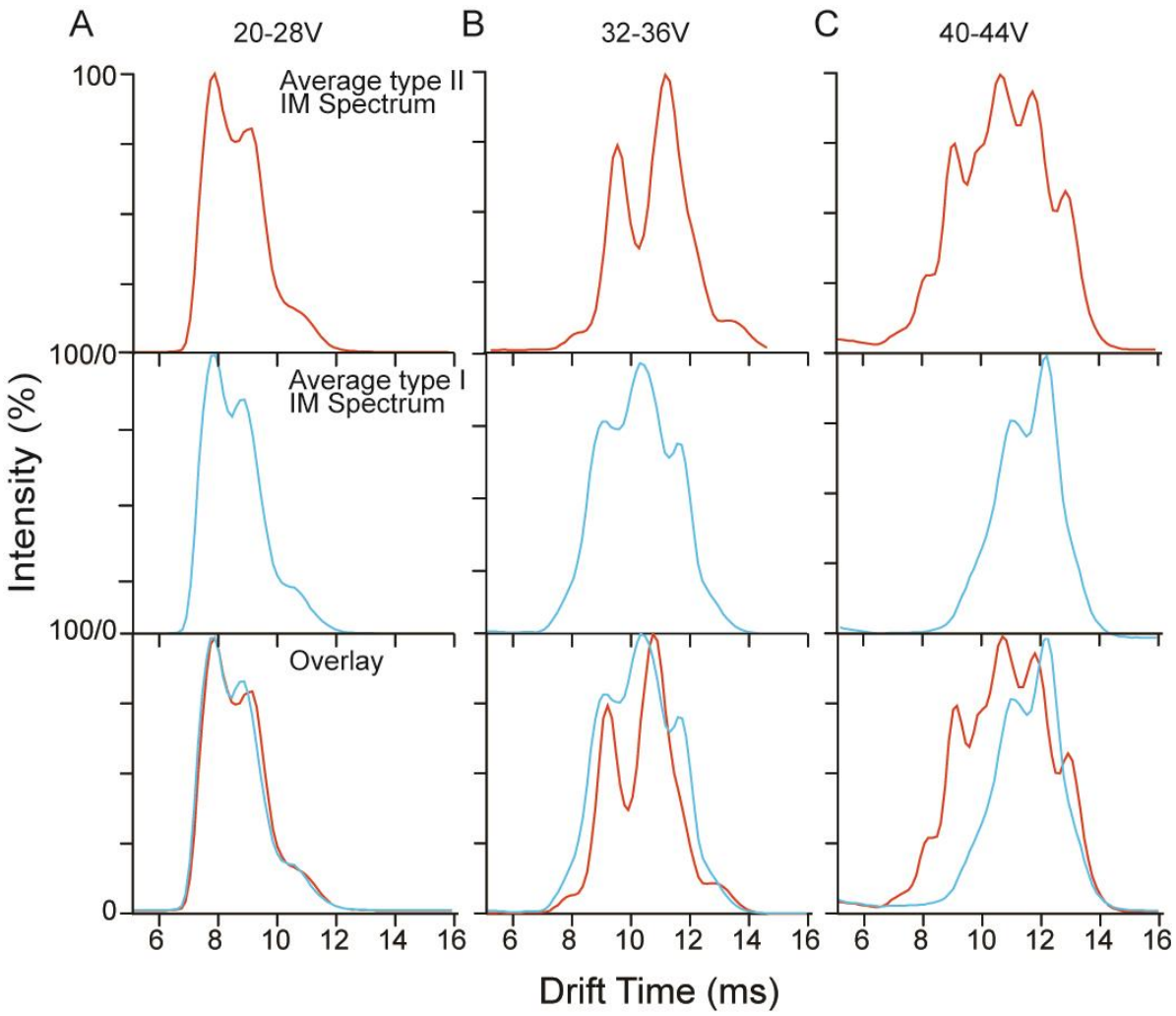

Figure S3. Averaged IM Spectra generated from all type I (blue) or type II (red) datasets are shown for selected regions of the CIU fingerprints recorded. Type II data is shown across the top of the diagram, with type I below and the two datasets are overlaid across the bottom. The integrated areas include (**A**) 20-28V, (**B**) 32-36V, and (**C**) 40-44V. The data shown in (**C**) is evaluated to have the highest discriminating power of those compared here and most useful for inhibitor screening. The features observed are discussed in more detail in the text.

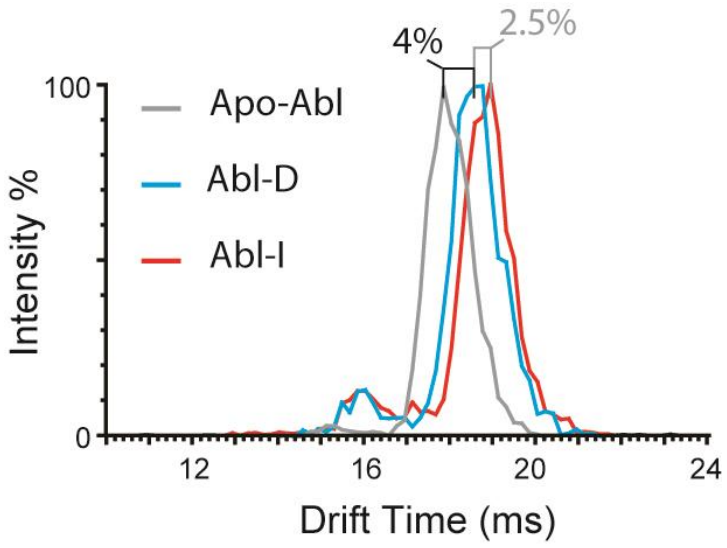

Figure S4. Ion mobility spectra for three samples. Apo-Abl kinase (grey), Abl bound to dasatinib (type I inhibitor, blue) and Abl bound to imatinib (type II inhibitor, red). There is a 4-6% difference in drift time between apo and holo forms of Abl, and a much smaller, but measurable drift time difference (2.5%) between the two bound forms.

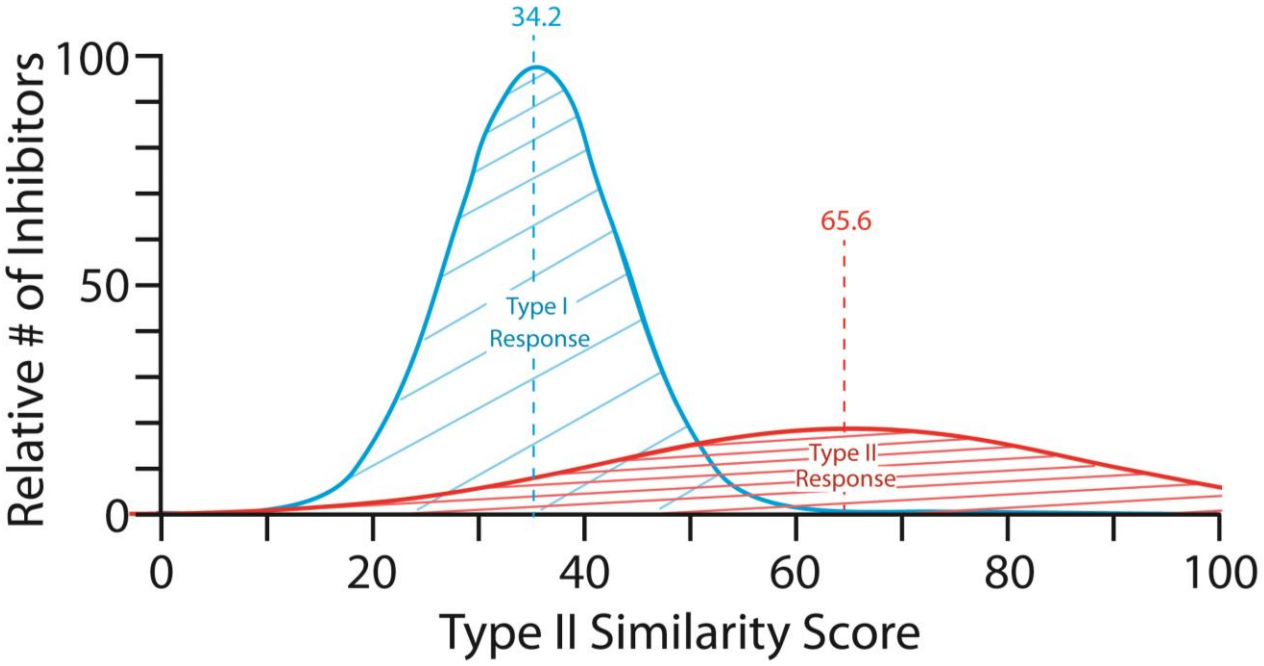

Figure S5. An illustration using the scores from Table 1, this graph uses the average and standard deviations of the recorded similarity scores to plot the normal distributions for the scores expected for these two classes of inhibitors if the observations made here hold for a larger screen (~1800 total compounds, 50% type I, 50% typle II simulated here). Average values are shown on the plot for Type I (blue) and Type II (red) inhibitors.

Figure S6. ATP K_m Curve of Phosphorylated c-Abl

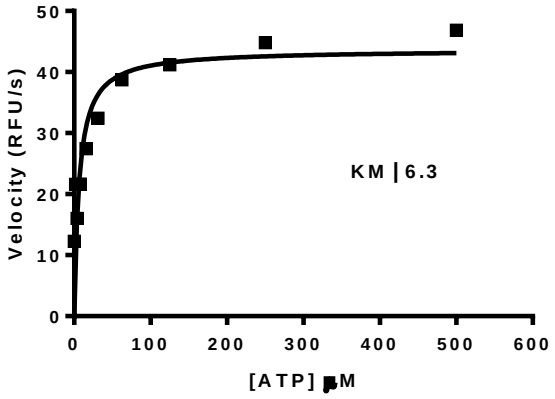

K_m = 5.9 ± 1.5 µM
rel. V_{max} = 38 ± 4.7 RFU/s

Figure S7. ATP K_m Curve of Non-Phosphorylated c-Abl

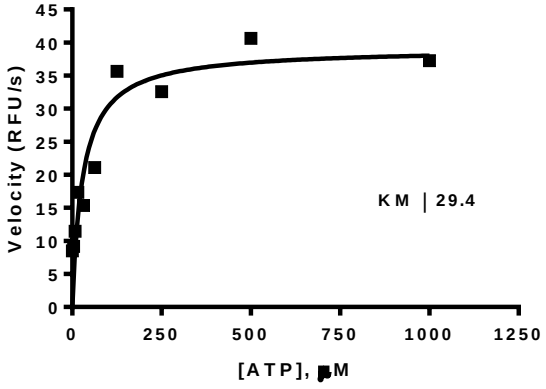

K_m = 22 ± 7.0 µM
rel. V_{max} = 45 ± 4.2 RFU/s

Analytical data for K_i determination. Each inhibitor K_i value was determined using at least 3 independent measurements. An example curve is provided for each inhibitor (**Figure S8, S9**).

Non-Phosphorylated c-Abl Data (Figure S8):

A) Bosutinib

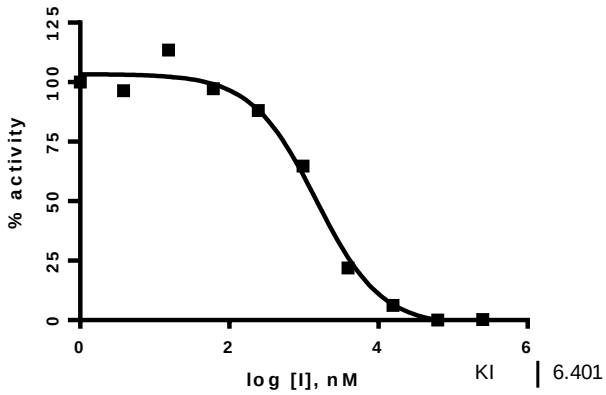

Avg K_i = 6.7 ± 1.0 nM

B) Dasatinib

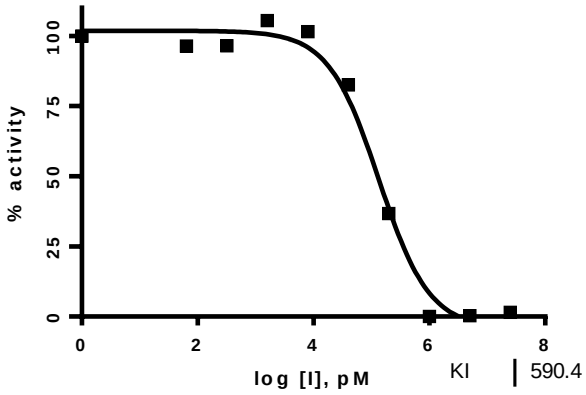

Avg K_i = 628 ± 42.0 pM

C) DCC-2036

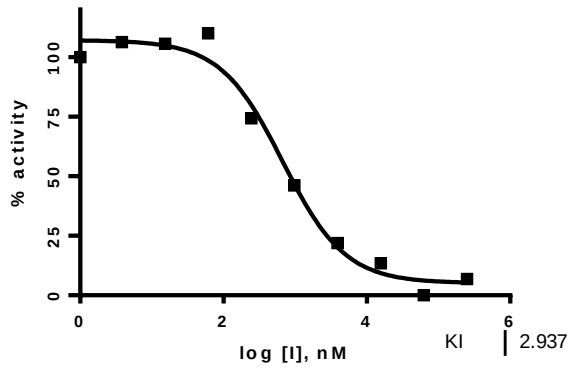

Avg K_i = 2.69 ± 0.3 nM

D) Imatinib

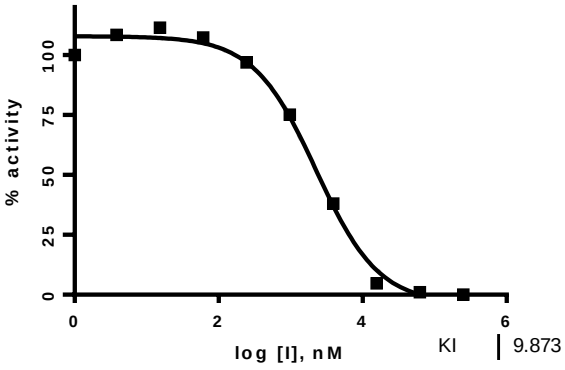

Avg K_i = 9.67 ± 0.19 nM

E) Nilotinib

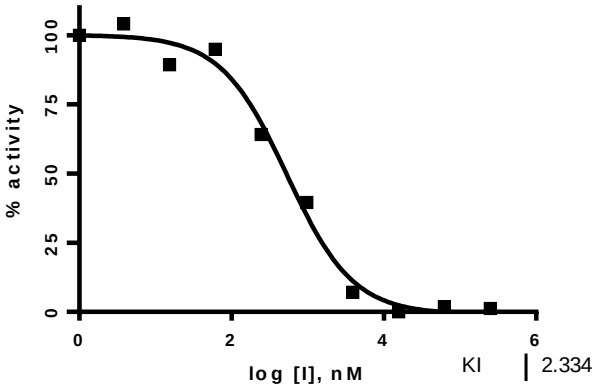

Avg K_i = 2.65 ± 0.24 nM

F) PP2

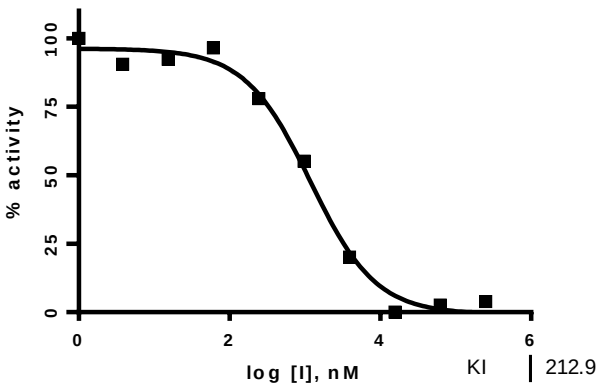

Avg K_i = 220 ± 5.11 nM

G) Saracatinib

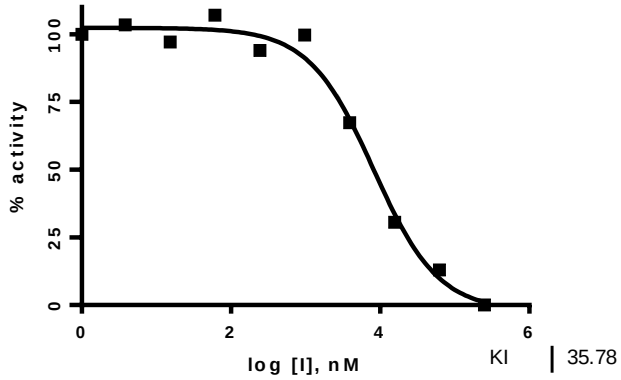

Avg K_i = 38.9 ± 4.24 nM

H) Staurosporine

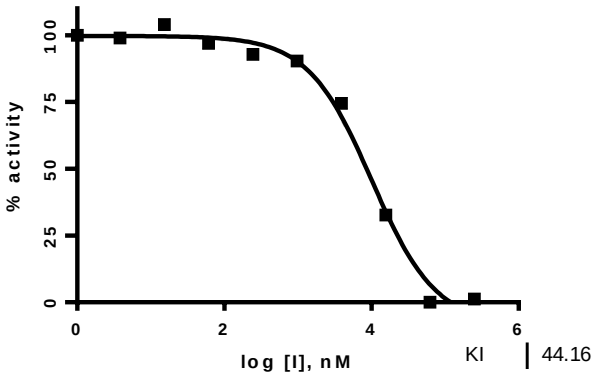

Avg K_i = 47.3 ± 2.54 nM

I) Tozasertib

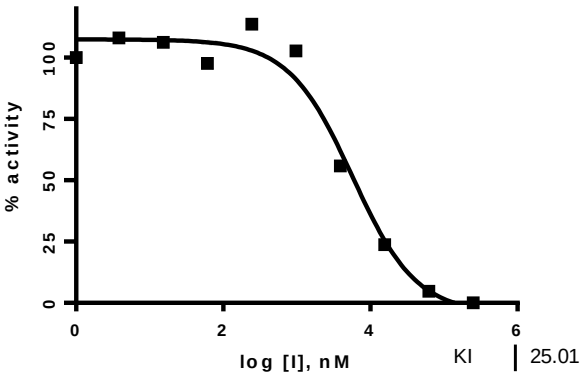

Avg K_i = 26.7 ± 3.74 nM

Phosphorylated c-Abl Data (Figure S9):

A) Bosutinib

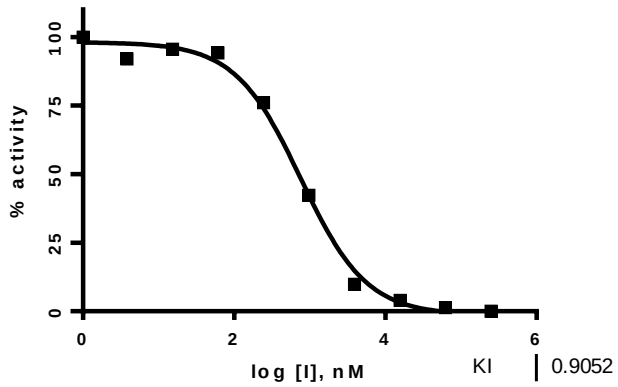

Avg K_i = 0.83 ± 0.14 nM

B) Dasatinib

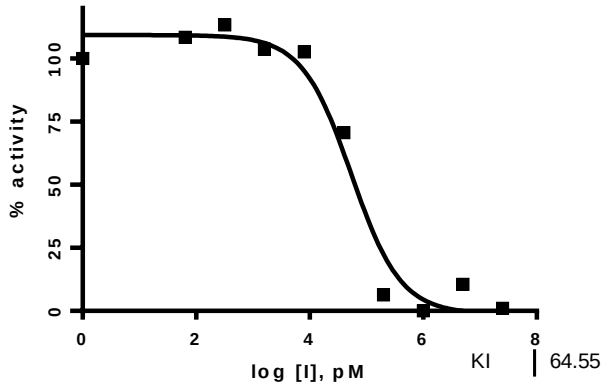

Avg K_i = 82.3 ± 14 pM

C) DCC-2036

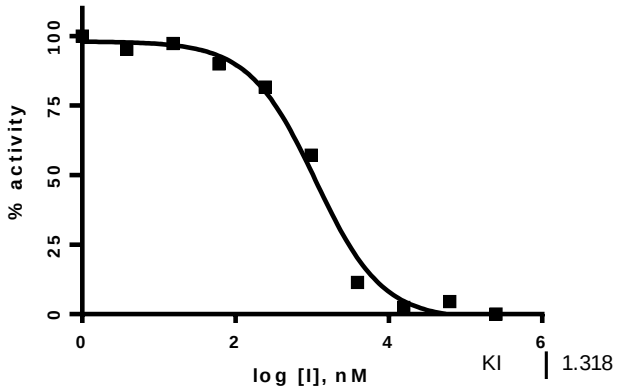

Avg K_i = 281 ± 56 nM

D) Imatinib

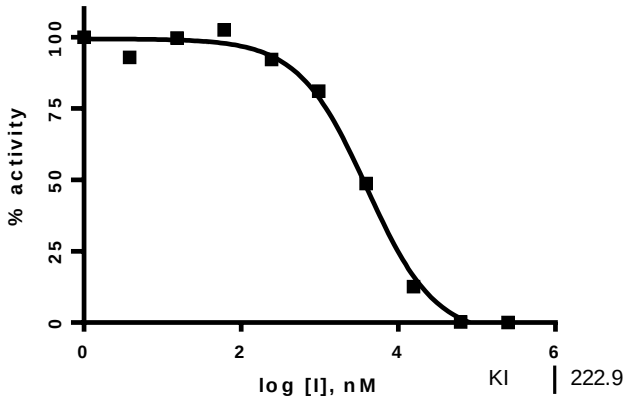

F) PP2

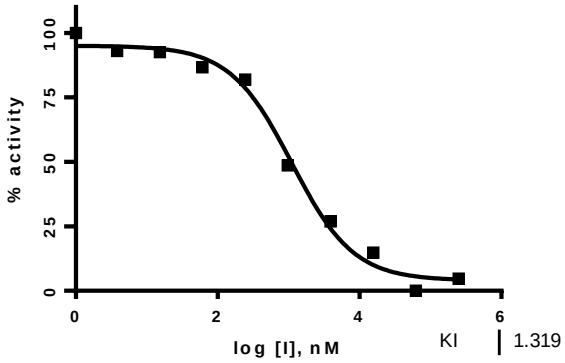

Avg K_i = 1.41 ± 0.40 nM

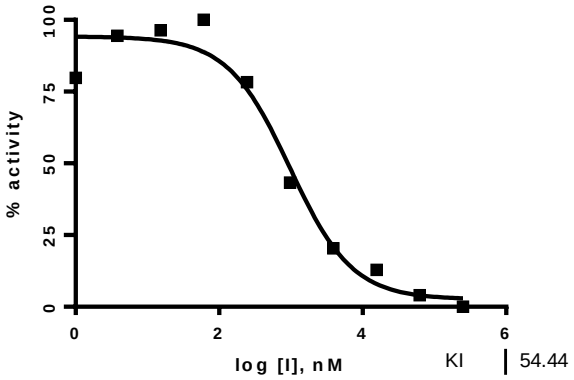

Avg K_i = 52.6 ± 1.3 nM

G) Saracatinib

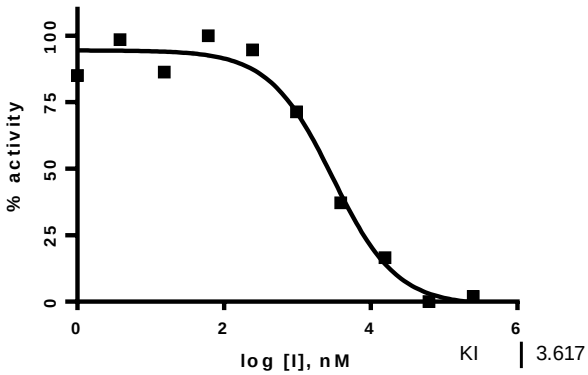

Avg K_i = 4.23 ± 1.31 nM

H) Staurosporine

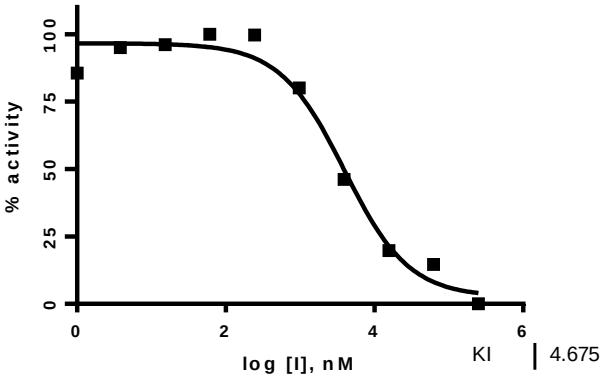

Avg K_i = 7.00 ± 1.83 nM

I) Tozasertib

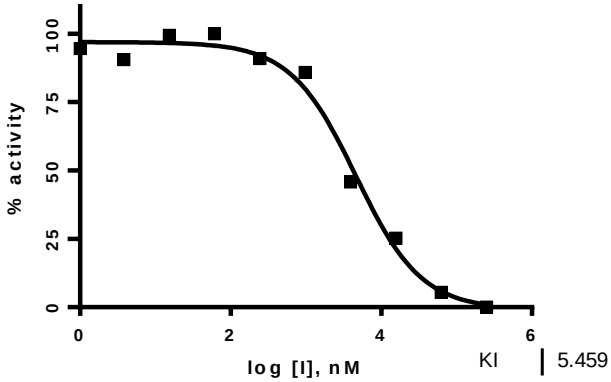

Avg K_i = 4.47 ± 0.70 nM

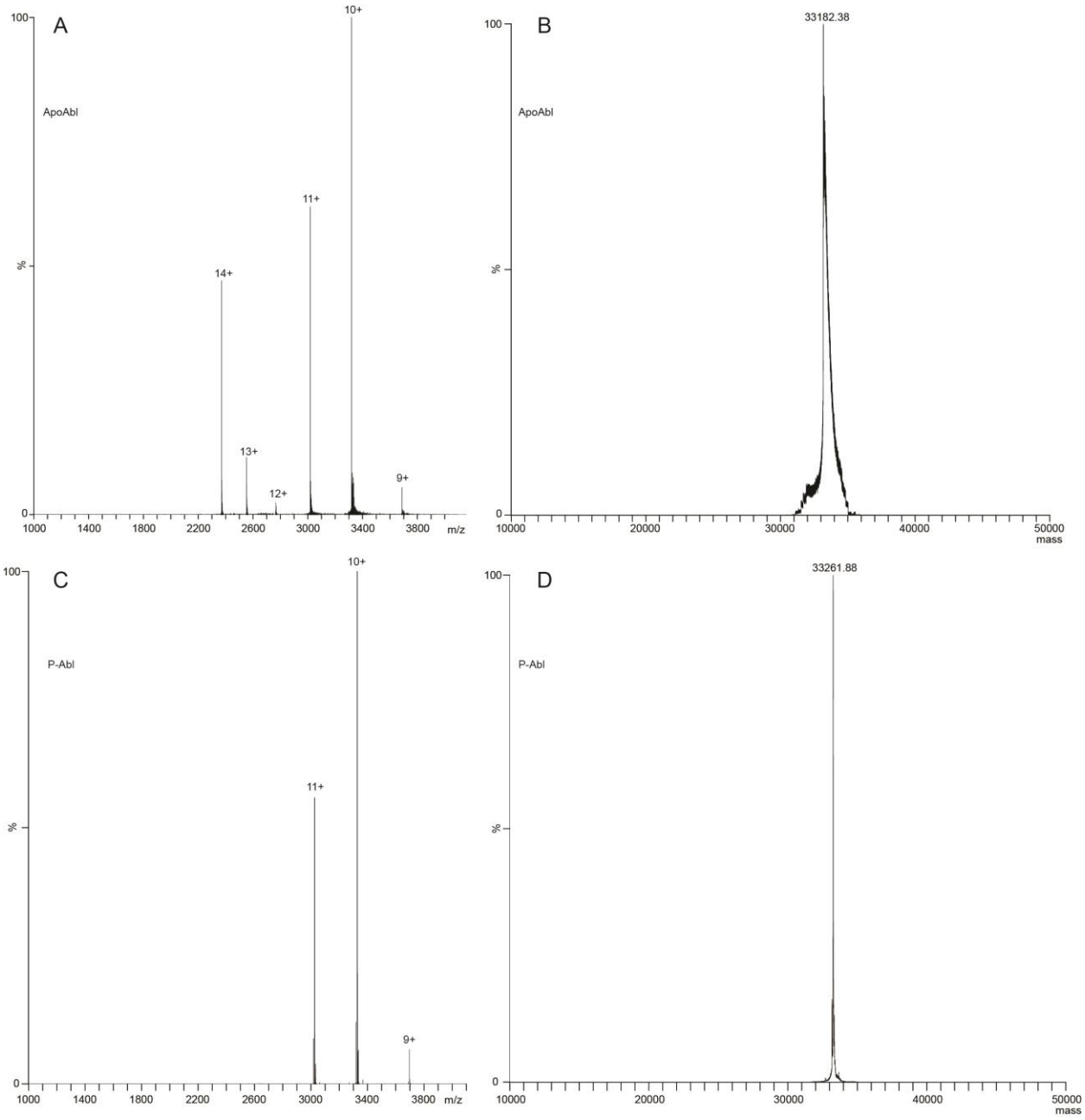

Figure S10. Mass Spectra of ApoAbl (A, B) and phosphorylated Abl (P-Abl, C,D). A) Mass spectrum of ApoAbl. B) Deconvoluted mass of ApoAbl. C) Mass spectrum of P-Abl. D) Deconvoluted mass of P-Abl. The recorded average mass difference between the two forms is 79.52 +/-0.90Da, indicating complete mono-phosphorylation of the P-Abl protein sample.